Relating SERS Intensity to Specific Plasmon Modes on Sphere Segment Void Surfaces

Sumeet Mahajan,[†,‡] Robin M. Cole,[‡] Bruno F. Soares,[‡] Suzanne H. Pelfrey,[†] Andrea E. Russell,[†] Jeremy J. Baumberg,*[,‡] and Philip N. Bartlett*[,†]

School of Chemistry, University of Southampton SO17 1BJ, U.K., and Cavendish Laboratory, University of Cambridge, JJ Thomson Avenue, Cambridge CB3 0HE, U.K.

Received: January 22, 2009; Revised Manuscript Received: March 17, 2009

Colloidal-crystal templated electrodeposition can be used to fabricate sphere segment void (SSV) substrates that show large, reproducible enhancements in surface-enhanced Raman spectroscopy (SERS). These SSV substrates support a variety of plasmon modes and can be fully characterized by white light dispersion measurements allowing the direct identification of the modes predicted by computational models of the nanoscale optical fields. Comparing plasmon absorption with SERS enhancements as a function of sphere segment void diameter and metal thickness for a series of SSV substrates allows the identification of the specific plasmon modes, which give rise to large SERS enhancements at different laser wavelengths and in different media. The measured SERS intensities show direct correlation to the plasmonic modes of the structures providing a guide to the design of efficient surfaces for SERS.

Introduction

The discovery of intense Raman signals on roughened silver surfaces[1] and the recognition that this was due to a local electric field enhancement process[2,3] significantly excited the scientific community. However, the initial promise of surface-enhanced Raman spectroscopy has largely remained undelivered due to its irreproducibility, which has stemmed from the lack of reproducible substrates. Over the last three decades, tremendous progress has been made toward fabricating reproducible SERS active substrates,[4] as well as toward a theoretical understanding of the mechanism of SERS. However, further improvements are needed to gain universal acceptance of SERS techniques and the wide scale development of commercial analytical applications. Recent advances have been accompanied by considerable debate on the origin of SERS enhancement over the last few decades.[5−8] It is now widely accepted that the principal contribution to the observed signal enhancement is due to intense local electric fields associated with surface plasmon polaritons (SPPs; henceforth referred as plasmons). For the conventional 10^6-10^8 average SERS enhancement, chemical enhancement contributes a factor of around 10−100 while the remainder is due to electromagnetic field enhancement by plasmons.[9] However, a comprehensive understanding of the role of different types of plasmons in the enhancement process is emerging only now.

We have developed a cost-effective methodology of templated electrodeposition through self-assembled polystyrene spheres[10] for fabricating sphere segment void (SSV) substrates. The SSV substrates can be fabricated reproducibly and have been produced from a wide range of materials including metals,[10,11] semiconductor oxides,[12] and conducting polymers.[13] These substrates have been shown to possess interesting magnetic,[14] superconducting,[15] wetting,[16] and optical properties[17] arising from the unique patterned geometry. The substrates have widely tunable optical properties as a result of the dual control offered by the choice of sphere diameter and electrodeposited thickness of the film and have been studied in detail both experimentally[17] and theoretically.[18,19] Since coinage-metal substrates support plasmons, they generate intense electric fields under illumination and consequently show huge enhancements of SERS[20−22] and SERRS[23] in air as well as electrochemically modulated SERS in solutions.[24,25]

Understanding the precise plasmonic characteristics of the SSV substrates is of primary importance to the investigation of the SERS enhancement process and for using it in real applications. We have shown that SSV substrates support a wide variety of plasmon modes which can be engineered with great precision. By tailoring the structure geometry it has been possible to optimize the substrates for SERS in the UV[26] or even in the near-infrared (NIR).[20] The various observed plasmon modes correspond to both localized and propagating electromagnetic fields that can be excited by incident light and are localized to different extents at the surface of the metal. Using the SSV structure, plasmons can be locally trapped producing significantly enhanced optical fields at precise locations. Such SSV surfaces combine the easy coupling of a spherical geometry embedded in a film with the field-focusing ability of sharp tips in a very controllable and reproducible way, in contrast to studies involving either metallic nanoparticles in close proximity or sharp metal tips brought close to a smooth surface as reported elsewhere.[27,28] The contrasting properties of nanoparticles and SSV substrates, compared in Figure 1, essentially depend on how the opposite curvature of their metal surfaces modifies the field energies; calculations show that the SSV geometry supports radically different plasmon modes to metal particles or tips.[29] For SSV structures, charge distributions on the walls of the void cavity provide the electric field distributions which constitute the plasmon modes. Since the fields are concentrated inside the dielectric cavity (as opposed to around the metal of a nanoparticles system), there is reduced damping in the void structure. The field enhancement depends on the contribution of both reradiation (optical loss) and damping (absorption loss) and in these nanovoids is found to result in longer plasmon confinement

* To whom correspondence should be addressed. E-mail: jjb12@cam.ac.uk; pnb@soton.ac.uk.
[†] University of Southampton.
[‡] University of Cambridge.

10.1021/jp900661u CCC: $40.75
Published on Web 04/30/2009

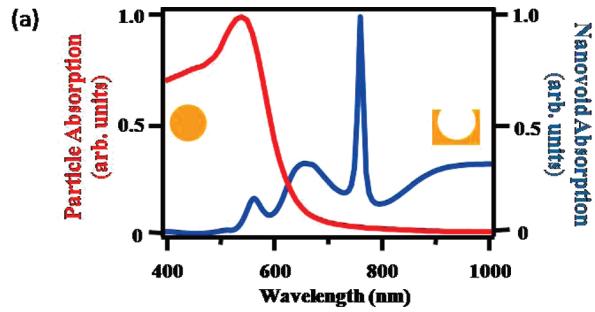

(b)

	Particle	Sphere Segment Void
SEM	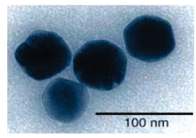	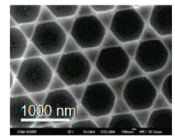
Electric field intensity distribution	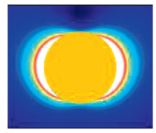	
Max E^2 Enhancement	< 30x	< 60x
Distance dependence	r^{-12} from dipole resonance, <10nm	Intense electric fields up to 100nm off metal surface
Coupling efficiency	Complex scattering by particle array	Up to 98% from ordered void array
Reproducibility	Irreproducible, 'hot spots'	better than 5%, due to well ordered structure
Useable particle size range (Au)	10-100nm: high energy modes ~ ω_p	100nm-μm: modes 0.5eV to ω_p

Figure 1. (a) Absorption cross-section calculated using a boundary element method for (red) 50 nm diameter Au particle and (blue) 600 nm diameter cavity in Au, normalized to the peak absorption. (b) Comparison of particle[30] (for r^{-12} dependence, see ref 31) and void properties. Electric field intensity distributions show that the SSV geometry supports radically different plasmon modes to metal particles. The negative curvature of the cavity surface (yellow) pushes the electric field out of the metal; the color scale corresponds to zero field (blue) to intense field concentration (white). Localized plasmon modes are not supported for frequencies above the plasmon frequency ω_p.

times (giving narrower plasmon linewidths than for nanoparticle plasmons) and therefore stronger excitation of molecules for SERS.

The wide wavelength tunability of the plasmon modes makes these substrates ideal for quantitatively studying SERS enhancement, where fields are required at both the incoming and outgoing SERS wavelengths. Larger (micron diameter) SSV substrates typically support many higher order plasmon modes, each with unique field structures allowing the investigation of SERS from molecules at several distinct locations within a single geometry. Furthermore, the open SSV geometry can be wetted, allowing the study of SERS in solution.[25,32] The wide plasmonic tunability of SSV substrates compares favorably with the nanoparticle-based nanotriangle and AgFON films[33] which are fabricated by vacuum deposition. The SERS enhancements of these nanoparticle-based substrates has been identified from correlation with the spectrally broad localized surface plasmon resonances (LSPR) from "hot" spots.[34] The plasmonic resonances on SSV substrates are spectrally narrow and can be simply tuned by the structure geometry, allowing the precise correlation between structure extinction and SERS enhancement to be extracted.

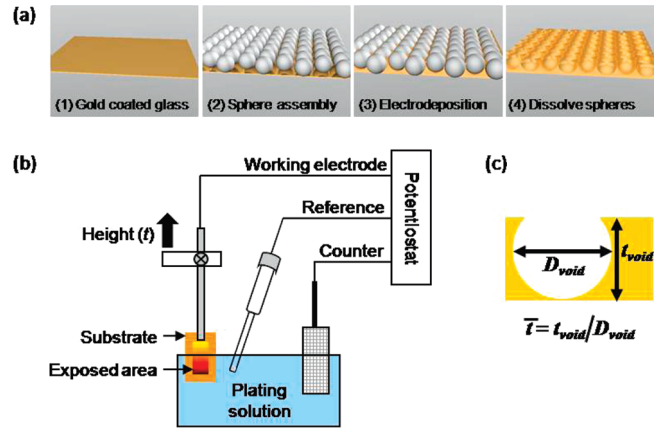

Figure 2. (a) Schematic of self-assembly and electrodeposition procedure for fabricating SSV substrates. (b) Schematic of the electrochemical setup for preparing graded substrates. Working electrode and substrate are progressively withdrawn to obtain a sample with a gradation of thicknesses, with the thinnest film at the top and thickest at the bottom of the sample. A delimited rectangular area of the template is left exposed while masking the remaining area with an insulating varnish. A saturated calomel electrode is used as the reference and a platinum mesh as the counter. (c) Definition of normalized thickness $\bar{t}$.

Here, we present a comprehensive investigation of the SERS obtained on SSV substrates and the plasmon modes responsible for the enhancement. The plasmon modes are fully characterized using angle-resolved white light dispersion measurements and the local electric fields calculated using a computational boundary element method (BEM).[29] In contrast to the AgFON substrates, where a single SERS enhancing plasmon mode is present, we investigate the SERS enhancement from several different coexisting plasmon modes, each of which can be tuned in wavelength by altering the cavity size while maintaining the electric field intensity distribution of the mode. Since SSV substrates prepared by electrodeposition are essentially electrodes they are suitable for electrochemical SERS investigations.[24,25] SSV substrates have been shown to produce stable and reproducible signals with SERS active molecules under solutions and are ideal for developing analytical tools for diagnostics and healthcare where applications in fluids are essential.[32] However, substrates should be optimized for the medium in which they have to function, necessitating control over mode energies and electric field distribution in solution, a consideration less well studied in the SERS community. Here, SERS enhancements are characterized for a wide range of laser excitation wavelengths in both air and solution.

Experimental Section

Fabrication of SSV substrates is by a two-stage self-assembly and electrodeposition process, shown in Figure 2. Substrates for templated electrodeposition were prepared by evaporating 10 nm of chromium followed by 200 nm of gold onto 1 mm thick glass microscope slides. These substrates were extensively cleaned by sonication in 2-propanol, followed by rinsing in deionized water, and dried using argon. Cysteamine was then self-assembled on the surface by immersion in its 10 mM ethanolic solution at room temperature for at least 48 h. Colloidal polystyrene spheres were obtained as 1 wt % aqueous suspensions from Duke Scientific Corp. The deposition of colloidal templates (of sphere diameter from 350−1100 nm) was carried out in a thin-layer cell comprising the cysteamine-coated gold electrode and a clean, uncoated microscope cover glass held

100 μm apart by a spacer cut from Parafilm (Pechiney Plastic Packaging, Inc.). The filled thin-layer cell was placed in an incubator in order to control the rate of evaporation from the cell. Upon drying, the spheres self-assemble to form a monolayer of the colloidal crystal which appears opalescent, with colors ranging from red to green depending on the angle of observation, clearly visible when illuminated from above with white light. The template-covered surface was removed from the thin-layer cell, and electrochemical deposition was performed in a separate thermostated cell at room temperature using a conventional three-electrode configuration controlled by an Autolab PG-STAT30. The template-coated gold substrate was the working electrode with a large area platinum gauze counter electrode and a homemade saturated calomel electrode (SCE) as the reference. Gold was deposited from a commercial cyanide-free gold plating solution (ECF 60, Metalor). A plating additive (Brightener E3, Metalor) was added to the plating solution to give a smooth finish to the deposits. To obtain samples with a series of steps in SSV thickness (referred to as a graded sample), the fabrication scheme shown in Figure 2b was used. This allowed the systematic study of plasmons and SERS as a function of structure morphology on a single substrate. A rectangular portion of the template was left exposed by masking the rest of the area with an insulating varnish. A precalculated charge was passed through the template to obtain a particular thickness in a potentiostatic electrodeposition pulse at -0.73 V versus SCE. The template was withdrawn from the electroplating solution in 1 mm steps, and the differential charge corresponding to the new thickness was passed. In this way, a sample with a systematic gradation of thicknesses was obtained with the thinnest film at the top and the thickest at the bottom. Following electrodeposition, the polymer spheres were removed by dissolution in DMF. This resulted in substrates with an array of interconnected spherical cavities, shown in Figure 2 (part a4).

SSV substrates support both localized and propagating surface plasmons. Propagating surface plasmons have energies that depend on the incident angle of light, whereas localized plasmons have an energy independent of the incident angle.[19] Thus, angle-resolved spectroscopy is the key to distinguishing the plasmons on such surfaces. An automated goniometer allows the full spectral and angular dispersion of the plasmon modes to be mapped with high spatial resolution for direct comparison with SERS spectra. Although not presented here, the full angle-resolved dispersion data allows the precise identification and labeling of plasmons modes. Absorption "maps" showing absorption spectra at each film thickness are constructed from the angle resolved measurements performed on the goniometer. Spectra are integrated over a range of incident angles from $0-30°$, allowing the direct comparison with SERS results obtained using microscope systems, typically with x50 (ULWD, NA:0.5) objectives. The maps show log(reflectivity) as color plots, where black corresponds to 100% reflected light and yellow corresponds to 0% reflectivity. A cell was constructed to allow these measurements to be performed in solution, and the same cell was used for the SERS measurements. By comparing these maps to equivalent simulations of the absorption and near-field profiles of the structure, it is possible to identify the precise plasmon modes responsible for the SERS enhancements. Calculations are performed using a boundary element method (BEM), where the field inside a single isolated cavity is expressed in terms of the charges and currents of the structure surface (for full details see ref 29).

Benzenethiol was used as the SERS probe molecule; it was adsorbed onto the substrate by immersion in a 10 mM ethanolic solution for at least 1 h and thereafter thoroughly washed with ethanol. The absence of the S−H bond vibration at 2566 cm^{-1} indicates that the thiol is attached to the surface and that the coverage does not exceed one monolayer. SERS measurements were carried out on graded samples using laser wavelengths of 633, 785, and 1064 nm. Raman spectra with a 633 nm laser were recorded with a Renishaw 2000 Raman microscope. Raman spectra with the 785 nm laser were recorded on a Perkin-Elmer RamanStation 400. Finally, Raman spectra with a 1064 nm laser were acquired with a Perkin-Elmer System 2000 FT-Raman instrument. SERS spectra were recorded at uniformly spaced intervals along the length of graded samples for sphere diameters from 350 to 1100 nm. The peak intensities in the work presented here have been calculated after subtracting the background from the spectra.

Results and Discussion

A single graded SSV substrate can exhibit intense SERS enhancements over a wide range of wavelength excitations at the same or multiple locations on the substrate, as selected by the thickness of the layer, which determines the surface morphology. The SERS signal for benzenethiol adsorbed on a graded 600 nm sphere-diameter Au SSV substrate is plotted as a function of film thickness and overlaid on the corresponding absorption map in Figure 3a. The intensity of the 1571 cm^{-1} Raman scattered peak, corresponding to the ring stretching mode of benzenethiol, is extracted after background subtraction and plotted for each laser wavelength (SERS intensity is plotted as the marker size for each film thickness). The absorption profile reveals several distinct modes, which tune rapidly in frequency with increasing thickness of metal. Maximum SERS enhancements are observed when the incident laser is in resonance with a plasmon mode. The broad line width of these modes ensures that the plasmon fields and molecules excited are identical at the incoming and outgoing photon wavelengths, a condition clearly required for maximum SERS enhancement.

To further elucidate the origin of the plasmon resonances, the theoretical absorption and corresponding plasmon local fields for this substrate are presented in Figure 3b for one sample thickness. Detailed calculations[29] reveal that these modes can be described as the $1P_+$ (bonding) and $1P_-$ (antibonding) *mixed* state between the 1P cavity mode and a dipole rim mode which exists across the spherical opening to the cavity. In a fully encapsulated void, the P cavity mode is the lowest order mode of the system, possessing a spherically symmetric electric field distribution provided by charge nodes at the top and bottom of the void. On truncation of the cavity this mode splits into different azimuthal m components due to symmetry breaking of the system. The 1P identified mode indicates that it possesses an $l = 1$ angular symmetry and $m = 1$ azimuthal symmetry and is dipole-like (similar to Y_{lm} atomic orbitals). The $1P_+$ mode possesses a field distribution aligned *across* the cavity, with charge nodes located within the rim, and a field distribution in the *plane* of the rim. This mode provides a strong field enhancement directly at the metal rim as well as a significant field enhancement at the center of the cavity opening, shown in Figure 3b. The $1P_-$ mode also has a strong field component at the metal rim, but the void mode and rim contributions have field components aligned in antiphase; in this case, the void field component is forced deeper into the void, as shown in Figure 3b. A comprehensive description of these modes is presented in ref 29. Therefore, these modes support intense fields

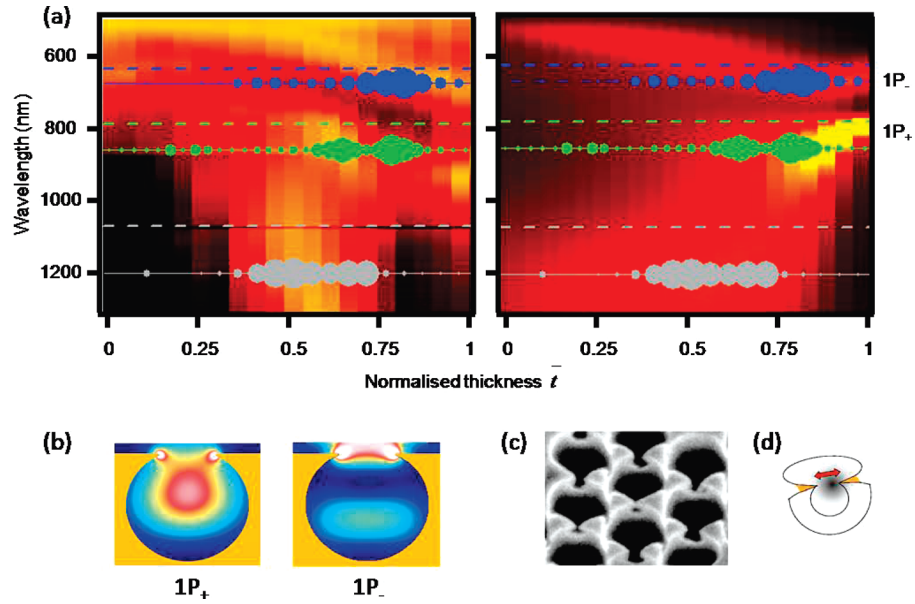

Figure 3. (a) Experimental (left) and calculated (right) 600 nm SSV position resolved absorption maps are integrated over a range of incident angles from 0 to 30° for direct comparison with SERS measurements taken on a microscope. The peak SERS signal for laser wavelengths of 633, 785, and 1064 nm is overlaid on each plot. The bright areas indicate absorption. Dashed lines are incident laser wavelength, and solid lines are for the 1571 cm^{-1} Raman peak of benzenethiol at their absolute wavelengths red-shifted from the laser. The size of the circles is proportional to the intensity of the SERS peak and is relative to each other only for each respective laser excitation. (b) Fields of identified modes. The maximum E-field enhancement for the $1P_+$ mode is 60 while for the $1P_-$ mode it is about 3 times weaker. (c) SEM showing experimentally realized structure and (d) schematic of the tip mode.

located directly at the metal rim which are strongly coupled to incident light and provide efficient excitation of molecules at the surface for SERS. However, the calculations are for a single isolated void (as a truncated sphere array remains intractable), which leads to several key differences between the calculated and experimentally realized absorptions. First, in the experiment the periodic array of voids supports highly delocalized surface plasmons which are coupled by Bragg diffraction. These modes contribute to absorption for structures with normalized thickness, $\bar{t}$, less than 0.5, but do not give rise to SERS as seen in Figure 3a. Second, for graded experimental samples, SEM images reveal windows between neighboring voids that give rise to a tip structure seen in parts c and d of Figure 3, not accounted for in the simulations. This tip structure supports a low energy dipole mode which is seen to rapidly tune to IR wavelengths with increasing sample thickness. Coupling of this low energy mode to the $1P_+$ and $1P_-$ slightly enhances the optical fields but is beyond the scope of the current paper.

These results highlight the fact that SERS enhancement does not necessarily correlate to absorption by plasmons but has a complicated dependence on both the geometry of the SSV surface and the plasmon field profile. Only fields normal to the metal surface give rise to absorption by the metal; however, there are scattered and radiated components to the extinction measurements of SSV substrates which contribute to SERS enhancement.[35] A balance is expected between more radiative modes which have better out-coupling of the inelastically scattered plasmons, compared to more localized modes which have larger plasmon field confinement at the metal-molecule interface. Experiments reveal that absorption is indeed by far the greatest contribution to extinction by these structures, and indeed we see good correlation with SERS in Figure 3a. While quantitative comparison of the enhancement due to different modes at the same position on a sample is complicated by the different efficiencies of the three very different Raman spectrometers employed in this study, we find that similar SERS enhancements are found for each plasmon type (except for delocalized plasmons which, as noted above, show little SERS enhancement). This is broadly confirmed by our simulations which track the optical field averaged around the metal surface and the input and output plasmon coupling. Hence, for these substrates, all the localized plasmon resonances are effective in providing efficient SERS.

Since the plasmon modes and corresponding SERS enhancements tune as a function of sphere diameter and metal height, it is possible to systematically investigate and identify the optimum structure for SERS at a particular excitation wavelength. SERS from benzenethiol molecules was investigated on SSV substrates with sphere diameters from 350 to 1100 nm. The extracted SERS peak intensity of the 1571 cm^{-1} band of benzenethiol recorded with a 633 nm laser is plotted as a function of thickness and overlaid on absorption maps for substrates templated with 400, 500, 600, and 800 nm diameter spheres, shown in Figure 4a,c,e,g. Again, maximum SERS enhancement is observed when the incident laser is in resonance with a plasmon mode. Both the $1P_+$ and $1P_-$ modes (highlighted with triangles to guide the eye) are seen to give significant SERS enhancements. Variations in the position dependence and final energies of these modes are due to variation in gradation of the samples. Further modes not explicitly highlighted have been identified as both propagating surface plasmon modes below $\bar{t} = 0.5$, which again do not give rise to intense SERS, and higher order localized modes above $\bar{t} = 0.5$. It is clear from the results in Figure 4 that the same laser wavelength will produce strong SERS signals from a different (but potentially spatially overlapping) group of molecules on SSV samples with different thicknesses. This can be seen from the double resonance observed in Figure 4c,d,e,g when translating across the graded sample. The data also shows that resonance with plasmons either at the incoming laser or at the outgoing scattered wavelength can be effective at producing SERS enhancements. Nevertheless, such spatial selection through choice of the nanostructured geometry and wavelength can potentially be discriminated by

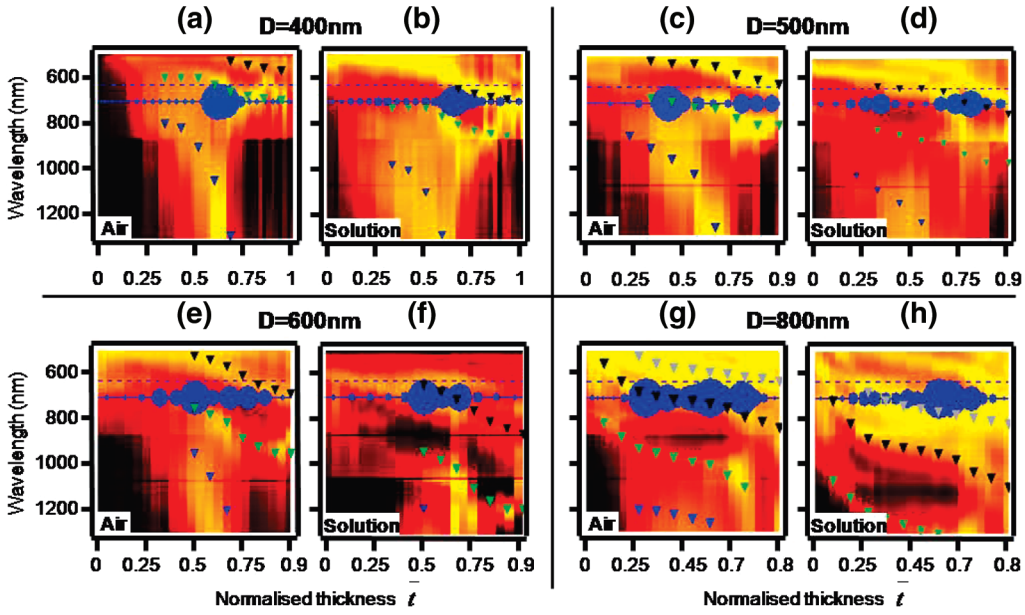

Figure 4. Position-resolved absorption maps with the SERS intensity overlaid for SSV substrates fabricated with various sphere diameters, D, recorded in air and water (a−h). The blue spot size corresponds to the background corrected peak intensity of the 1571 cm^{-1} band of benzenethiol. The dashed blue line indicates the 633 nm laser input. The plasmon modes indicated by triangles are as follows: (blue) low energy mode, (green) $1P_+$, (black) $1P_-$, (gray) 1D. The plotted plasmon mode energies are extracted in air and scaled for the solution refractive index.

selective tagging studies (ongoing) where molecules are attached in only specific regions of the nanostructure.

The SERS measurements were then repeated in water (Figure 4b,d,f,h) to obtain insight into in situ solution measurements.[32] Plasmon modes tune to longer wavelength with a shift proportional to the effective increase in refractive index at the metal/dielectric interface, here $n = 1.3$ for water. Upon wetting a given cavity, the plasmons tune in wavelength and different modes are now in resonance with the incident laser light, leading to different SERS intensity profiles with respect to position on the graded samples. Clearly, for the 400 nm diameter cavity the $1P_+$ mode is responsible for SERS enhancement in air, while the $1P_-$ mode produces the enhancement in water. Similar tuning is observed for the 500 and 600 nm samples, but for the 800nm sample, both the $1P_+$ and 1D modes contribute both in air and water. Recorded SERS signals (normalized to incident laser power and collection times) are always found to be 5−10 times stronger in air than in water. For comparison, experiments performed on a silicon wafer with a coverslip in water showed a 50% loss of Raman signal with the 633 nm laser and 25% loss with the 785 nm laser. Hence, the decrease in SERS intensities in water is not fully explained by either loss from the coverslip and aqueous cell used or in any change in damping of the plasmons (which should reduce as the modes tune to lower photon energy). Clearly, the observed decrease in SERS signals was many times more than the seemingly minor loss of the Raman peak of silicon in water. It is also not expected that the coupling strength of the SSV-localized plasmons would change since all plasmon modes on the surface tune similarly. A factor of 3 may be accounted for by the increased refractive index of water ($n = 1.3$) which reduces the electric field, reducing the SERS by n^4. We note that by changing the modes by choice of refractive index, we also collect SERS from different molecule populations within the void, contributing to changes in the SERS signal (as clear from the field profiles in Figure 3b). Figure 4 again confirms that a wide range of localized plasmons types give rise to SERS and that their enhancements can be easily manipulated by the choice of sphere diameter, metal height, and refractive index of the dielectric medium surrounding the voids. These results reveal that the optimum structure geometry for SERS enhancement is different for each laser wavelength. This has indeed been verified for key laser excitations used in SERS. It can also be seen from Figure 4 that for larger structures ($D = 800$ nm) localized plasmon modes do exist for structures of normalized thickness $\bar{t}$ less than 0.5, giving rise to SERS with a 633 nm laser. However, as the void diameter is increased further the fields near the surface are weaker due the higher order modes being supported at these energies. Furthermore, due to the range of optimum SSV geometries observed for SERS in different media necessitates engineering of structures for specific laser wavelengths, rather than using any specific rule of thumb.

Conclusions

We demonstrate the fabrication of reproducible sphere segment void (SSV) substrates by colloidal crystal-templated electrodeposition for surface-enhanced Raman spectroscopy (SERS) applications. SSV substrates support a variety of plasmon modes which scale with cavity dimensions and give rise to SERS enhancements of 10^6 or greater.[20,22,23] The plasmon modes are fully characterized by white light absorption measurements allowing direct identification of modes and comparison with computational models of the nanoscale electric fields responsible for SERS enhancement. Comparing plasmon absorption with SERS enhancements as a function of sphere size and metal thickness allows the identification of the optimum geometries for SERS at a range of different laser wavelengths and in different media. SERS signals show direct correlation to the plasmonic modes of the structures. SERS measurements repeated in solution, where the plasmons drop in frequency proportionally to the change in refractive index, again show maximal SERS enhancement when the incident laser light is in resonance with a plasmon mode; however, the signals are reduced by 1 order of magnitude; while we currently do not have a full explanation, the difference may be related to the enhancement of the SERS by coupling to different plasmon modes, which may sample different populations of the adsorbate

on the SSV surface. SERS is predominantly observed for samples of normalized thickness t greater than 0.5, since below this thickness plasmons are highly delocalized and less effective at feeding energy into surface-bound molecules. This approach to fabrication and characterization enables the engineering of plasmonic substrates with widely tunable plasmon modes for maximal SERS enhancement factors at any desired laser wavelength.

Acknowledgment. S.M. thanks ORSAS for a scholarship, and S.H.P. thanks Renishaw for sponsoring a CASE studentship. This work was funded under UK EPSRC grant EP/C511786/1.

References and Notes

(1) Fleischmann, M.; Hendra, P. J.; McQuillan, A. J. *Chem. Phys. Lett.* **1974**, *26*, 163.
(2) Albrecht, M. G.; Creighton, J. A. *J. Am. Chem. Soc.* **1977**, *99*, 5215.
(3) Jeanmarie, D. L.; Van Duyne, R. P. *J. Electroanal. Chem.* **1977**, *84*, 1.
(4) Wu, D.-Y.; Li, J.-F.; Ren, B.; Tian, Z.-Q. *Chem. Soc. Rev.* **2008**, *37*, 1025.
(5) Moskovits, M. *Rev. Mod. Phys.* **1985**, *57*.
(6) Moskovits, M. *J. Raman Spectrosc.* **2005**, *36*, 485.
(7) Campion, A.; Kambhampati, P. *Chem. Soc. Rev.* **1998**, *27*, 241.
(8) Otto, A. *J. Raman Spectrosc.* **2005**, *36*, 497.
(9) Schatz, G. C.; Young, M. A.; Van Duyne, R. P Electromagnetic Mechanism of SERS. In, *Surface-Enhanced Raman Scattering−Physics and Applications*; Kneipp, K., Moskovits, M., Kneipp, H., Eds.; Springer-Verlag: Berlin, 2006; Vol. 103, p 19.
(10) Bartlett, P. N.; Birkin, P. R.; Ghanem, M. A. *Chem. Commun.* **2000**, 1671.
(11) Bartlett, P. N.; Baumberg, J. J.; Birkin, P. R.; Ghanem, M. A.; Netti, M. C. *Chem. Mater.* **2002**, *14*, 2199.
(12) Bartlett, P. N.; Dunford, T.; Ghanem, M. A. *J. Mater. Chem.* **2002**, *12*, 3130.
(13) Bartlett, P. N.; Birkin, P. R.; Ghanem, M. A.; Toh, C.-S. *J. Mater. Chem.* **2001**, *11*, 849.
(14) Bartlett, P. N.; Ghanem, M. A.; El Hallag, I. S.; de Groot, P.; Zhukov, A. *J. Mater. Chem.* **2003**, *13*, 2596.
(15) Zhukov, A. A.; Filby, E. T.; Ghanem, M. A.; Bartlett, P. N.; de Groot, P. A. J. *Phys. C* **2004**, *404*, 455.
(16) Abdelsalam, M. E.; Bartlett, P. N.; Kelf, T.; Baumberg, J. *Langmuir* **2005**, *21*, 1753.
(17) Bartlett, P. N.; Baumberg, J. J.; Coyle, S.; Abdelsalam, M. E. *Faraday Discuss.* **2004**, *125*, 117.
(18) Kelf, T. A.; Sugawara, Y.; Baumberg, J. J.; Abdelsalam, M.; Bartlett, P. N. *Phys. Rev. Lett.* **2005**, *95*.
(19) Kelf, T. A.; Sugawara, Y.; Cole, R. M.; Baumberg, J. J.; Abdelsalam, M. E.; Cintra, S.; Mahajan, S.; Russell, A. E.; Bartlett, P. N. *Phys. Rev. B* **2006**, *74*.
(20) Mahajan, S.; Abdelsalam, M.; Suguwara, Y.; Cintra, S.; Russell, A.; Baumberg, J.; Bartlett, P. *Phys. Chem. Chem. Phys.* **2007**, *9*, 104.
(21) Baumberg, J. J.; Kelf, T.; Sugawara, Y.; Cintra, S.; Abdelsalam, M.; Bartlett, P. N.; Russell, A. E. *Nano Lett.* **2005**, *5*, 2262.
(22) Cintra, S.; Abdelsalem, M.; Bartlett, P. N.; Baumberg, J. J.; Kelf, T.; Sugawara, Y.; Russell, A. E. *Faraday Discuss.* **2005**, *132*, 191.
(23) Mahajan, S.; Baumberg, J.; Russell, A.; Bartlett, P. *Phys. Chem. Chem. Phys.* **2007**, *9*, 6016.
(24) Abdelsalam, M. E.; Bartlett, P. N.; Baumberg, J. J.; Cintra, S.; Kelf, T. A.; Russell, A. E. *Electrochem. Commun.* **2005**, *7*, 740.
(25) Abdelsalam, M.; Bartlett, P. N.; Russell, A. E.; Baumberg, J. J.; Calvo, E. J.; Tognalli, N. G.; Fainstein, A. *Langmuir* **2008**, *24*, 7018.
(26) Cui, L.; Mahajan, S.; Cole, R. M.; Soares, B.; Bartlett, P. N.; Baumberg, J. J.; Hayward, I. P.; Ren, B.; Russell, A. E.; Tian, Z.-Q. *Phys. Chem. Chem. Phys.* **2008**, *11*, 1023.
(27) Danckwerts, M.; Novotny, L. *Phys. Rev. Lett.* **2007**, *98*, 026104.
(28) Stockle, R. M.; Suh, Y. D.; Deckert, V.; Zenobi, R. *Chem. Phys. Lett.* **2000**, *318*, 131.
(29) Cole, R. M.; Baumberg, J. J.; Garcia de Abajo, F. J.; Mahajan, S.; Abdelsalam, M.; Bartlett, P. N. *Nano Lett.* **2007**, *7*, 2094.
(30) Kawata, S.; Masuhara, H. *Nanoplasmonics: From Fundamentals to Applications*; Elsevier Science & Technology: Osaka, 2004.
(31) McCall, S. L.; Platzman, P. M.; Wolff, P. A. *Phys. Lett.* **1980**, *77A*, 381.
(32) Mahajan, S.; Richardson, J.; Brown, T.; Bartlett, P. *J. Am. Chem. Soc.* **2008**, *130*, 15589.
(33) Lal, S.; Grady, N. K.; Kundu, J.; Levin, C. S.; Lassiter, J. B.; Halas, N. J. *Chem. Soc. Rev.* **2008**, *37*, 898.
(34) Haynes, C. L.; Van Duyne, R. P. *J. Phys. Chem. B* **2003**, *107*, 7426.
(35) Perney, N. M. B.; Baumberg, J. J.; Zoorob, M. E.; Charlton, M. D. B.; Mahnkopf, S.; Netti, C. M. *Opt. Express* **2006**, *14*.

JP900661U